Attenuating absorption contribution on Cn^2 estimates with a large-aperture scintillometer

Pierre Adrien Solignac, Aurore Brut, Jean-Louis Selves, Jean-Pierre Béteille, Jean-Philippe Gastellu-Etchegorry

Boundary Layer Meteorology
Springer Journals Editorial Office
Manuscript BOUN799R3
Accepted December 14, 2011

Attenuating absorption contribution on C_{n^2} estimates with a large-aperture scintillometer

Solignac*, P.A., Brut, A.*, Selves, J.L, Béteille, J.P., and Gastellu-Etchegorry, J.P.

CESBIO, 18, avenue Edouard Belin, bpi 2801, 31401 Toulouse Cedex 9

*Corresponding author, E-mail: pasolignac@gmail.com, aurore.brut@cesbio.cnes.fr

Abstract

Large aperture scintillometers (LAS) are often used to characterise atmospheric turbulence by measuring the structure parameter of the refractive index C_{n^2}. However, absorption phenomena can lead to an overestimation of C_{n^2}. By applying an accurate numerical filtering technique called the Gabor Transform to the signal output of a LAS, we improved our knowledge of the accuracy of the measured C_{n^2} by determining and attenuating the contribution of absorption. Two studies will be led on a 12-day dataset using either fixed band pass or adaptive filtering. The first one consists in evaluating the best-fitted filter for which the resulting C_{n^2} is independent of meteorological conditions, especially wind speed, and the second one consists in accurately attenuating absorption phenomena. A reference C_{n^2} (hereafter 'reconstructed C_{n^2}') will be created by accurately removing absorption from the scintillation spectrum, and will be used to evaluate each filter. By comparing the 'reconstructed C_{n^2}' with a raw C_{n^2} measured by a scintillometer we found that the average relative contribution of absorption to the measurement of C_{n^2} is approximately 1.6%. However, the absorption phenomenon is highly variable; occasionally, in the worst cases, we estimated that the absorption phenomenon could represent 81% of the value of C_{n^2}. Some explanations for this high variability are proposed with respect to theoretical considerations. Amongst the fixed band pass filtering used in this paper, we concluded on the preferential use of a band pass filter [0.2- 400 Hz] for C_{n^2}, as its performances are slightly affected by wind speed and that absorption contribution is reduced to 0.6%, with a maximal value at 60%. Using an adaptive filter on the 12-day dataset really improves the filtering accuracy on both points discussed in this paper.

Keywords: Absorption, Adaptive filtering, Atmospheric turbulence, Optical propagation, Scintillometer, Structure parameter of refractive index

1 Introduction

Scintillation phenomena are of interest to several scientific communities (e.g. astrophysics, optics, boundary layer meteorology). The twinkling effect (*i.e.*, rapid variations in the apparent brightness of a distant luminous object) can provide information on turbulent atmospheric characteristics for studies related to turbulent exchange of matter or energy. Additionally, scinillation also represents a disturbance or a source of error for studies related to optical measurements of light radiation within the atmosphere. This scintillation phenomenon can be explained as follows. The propagation of a wave through the atmosphere, defined as a turbulent medium, is affected by variations in the refractive index of air, n. These variations are due to fluctuations in humidity, temperature and pressure. Such turbulent effects can be described by the use of the structure parameter of the refractive index of air, C_{n^2} (Strobehn, 1968; Tatarskii, 1961).

The structure parameter C_{n^2} is measured using optical devices called scintillometers. Scintillometers are composed of a transmitter (*i.e.*, a light source) and a receiver. The transmitter emits an electromagnetic radiation through the atmosphere, and the receiver measures the intensity fluctuations of the propagating wave. Then the instrument computes the value of C_{n^2} from the variance of the logarithm of the signal amplitude, σ^2_{lnA}. The propagation path can be either vertical for C_{n^2} profiles and stellar optical system corrections (Avila et al. 1997; Vernin et al. 2009) or horizontal for surface flux estimation (de Bruin et al. 1995; Lagouarde et al. 2002) and terrestrial optical system correction (Ingensand 2002). Depending on the wavelengths of the light sources used by the transmitter, the measured fluctuations of the signal intensity can be sensitive to temperature or humidity effects. In this study, we only focused on optical scintillometers (that is, large-aperture scintillometres, or LAS) to measure C_{n^2} along horizontal paths. These instruments operate at near-infrared wavelengths of 880 nm or 940 nm, respectively (Kipp&Zonen, Scintec or Wageningen University & Research Centre, WUR), and they are mainly sensitive to temperature fluctuations, although humidity still slightly affects their measurements.

Using scintillometry requires some knowledge about the metrology of the instrument. The accuracy of a scintillometer (whether 880 nm or 940 nm) is sensitive to certain technical and theoretical criteria. For example, consider the case of the optical LAS (Wageningen University & Research Centre). Its aperture diameter is D = 0.15 m, and it operates at 940 nm. As such, the errors can be divided into the following categories:

- Electronics: This may imply an error up to 3% for low C_{n^2} (Moene et al. 2005) when considering the sum of the errors due to the miscalibration of the two log-amplifiers of the receiver.
- Path length calibration: This may imply an error of 2 - 4.5% (Moene et al. 2005) for distances between 1 km and 5 km.
- Optics alignment and focus of the mirror (Kleissl et al. 2009): This may imply an error of 2 mm in the effective diameter estimation, leading to a 4% error in C_{n^2}.

Other inaccuracies are related to the validity of theoretical assumptions, including the following issues.

- It is assumed that the scintillometer is sensitive to eddies that are in the inertial subrange of turbulence. The device is mainly sensitive to eddies of the size of its diameter, and then, in analysis, it is assumed that it is independent of the inner scale, l_0. The condition on the outer scale L_0 is then dependent on the set-up height, as the size of the outer scale is of the order of the height of the instrument.

- The contribution of absorption fluctuations is negligible.

This last assumption is the subject of this study. This work focuses on evaluating the impact of absorption on the measurement of C_{n^2} in a lossy atmosphere using a scintillometer with a source wavelength of 940 nm. The aim is to improve the accuracy on the C_{n^2} estimate with a limited number of theoretical assumptions. Therefore, this study is original as it deals with the experimental evaluation of the contribution of absorption to C_{n^2} measured by optical scintillometry.

Absorption and scintillation (or refraction) both contribute to the value of C_{n^2} measured by a scintillometer, but their influence occurs at different time scales. Scintillations are local phenomena, as most influent eddies are typically the size of the beam diameter, assuming that $D >> \sqrt{\lambda L}$, L is the transect length and λ is the operating wavelength. In contrast, absorption is a path-integrated process, so variations at larger spatial scales become the determining factor. Thus, absorption is stronger at low frequencies, whereas scintillation is more important at high frequencies. Therefore, when the absorption phenomenon is strong (and scintillation is weak), its effect on the scintillometer-measured signal leads to an overestimation of C_{n^2}. Although absorption influence is supposed to be negligible for estimations of C_{n^2} (Nieveen et al. 1998), experiments have already proven that this effect is very likely to affect measurements (Green et al. 2000; Hartogensis et al. 2003). For most scintillometers, the attenuation of the effect of absorption on the measured signal is usually performed by an analogue band-pass filter. The upper cut-off frequency is set at 400Hz to reduce noise coming from high frequencies, but do not infer with absorption removal. However, several authors have suggested different values for the low cut-off frequency of the band-pass filter. For optical scintillometers, the low cut-off frequency was first fixed at 0.03 Hz (Ochs and Wilson 1993), but Nieveen et al. (1998) suggested that this value be increased up to 0.5 Hz because of strong absorption at night. Then, after the La Poza experiments (Hartogensis et al. 2003), the low cut-off frequency of the filter was set to 0.1 Hz (McAneney et al. 1995; Meijninger et al. 2002; Moene et al. 2005). For industrial LAS, the lower cut-off frequency is currently fixed at 0.2 Hz (Kleissl et al. 2008) for instruments from Kipp&Zonen. Otherwise, the Boundary Layer Scintillometer (BLS) from Scintec uses a procedure to remove absorption based on the correlation function.

The aim of this study is first to understand and quantify the effect of absorption on the value of C_{n^2} estimated by an LAS with a source wavelength of 940 nm. Then, the filtering effect of these absorption phenomena will be discussed in terms of improvements of the C_{n^2} measurement. However, this implies to filter the scintillometer signal in order to remove the effect of the absorption fluctuations, without suppressing too much variance such that the actual scintillations would be underestimated. To achieve this objective, we chose to record the measured signal at the output of a scintillometer and to perform different kinds of filtering (band-pass filtering and adaptive filtering). Using this approach, we could attenuate the effect of absorption on the value of C_{n^2} and make conclusions regarding its contribution to the measurement of C_{n^2}.

So, eventually, the paper is structured according to the following plan. First, we present the collected dataset (turbulent fluxes from Eddy Correlation tower and scintillometer data). Then, some theoretical aspects of the scintillometer measurements, like the contribution of absorption to the C_{n^2} measurement or the wind speed effect on the turbulent spectrum, are presented and discussed using some analysis from the dataset results. Then, several filters are considered (fixed band pass and adaptative band-pass filtering) and evaluated in comparison with the theory. Then, we discuss the effects of the various filtering regarding to their capacity to remove the absorption fluctuations on a signal measured with a scintillometer.

2 Experimental set-up and dataset

The experiment took place over a maize field at Lamasquère, which is located 30 km southwest of Toulouse, France. The field is flat and almost homogeneous (Solignac et al. 2009a; Beziat et al. 2009). An LAS built at WUR was installed on a 6 m-high mast along a 565 m transect, between July 15th and August 24th 2008. The LAS features are as follows. The mirror diameter is D = 0.15 m, and the source wavelength is λ = 940 nm. The signal at the output of the detector of the scintillometer (*i.e.*, 'Detect' output) was processed by our own electronic devices (Solignac et al. 2007), where the processing included functions for demodulation and acquisition of the signal. This approach allows us to record the raw signal with no filtering using an optimised sampling frequency. In our case, the sampling frequency was set to 1 kHz according to both the maximum scintillation frequency (400 Hz) and the Shannon criteria.

In addition, the site, which belongs to the Carbo-Europe Network, is also equipped with an eddy correlation flux tower (3.65 m) at the mid-path of the transect (Beziat et al. 2009). It was set up in the year 2004 and is composed of:

- A CSAT 3 sonic anemometer (Campbell Scientific Inc, Logan, UT, USA) to measure 3D wind components and temperature;
- A Licor open path CO_2 (c) and H_2O (q) analyser (LI7500, LiCor, Lincoln, NE, USA);

Mis en forme : Exposant

Mis en forme : Exposant

- A Vaisala probe (HMP35A, Vaisala, Helsinki, Finland) for the relative humidity and temperature;
- An ARG100 rain-gauge (Environmental Measurements Ltd., Sunderland, UK) for measuring precipitation rates.

Sensible (*H*) and latent (L_vE) heat fluxes are calculated at a 30-min. timestep using the turbulent measurements (20Hz) of the Eddy Correlation tower. The data are processed according to the Carbo-Europe recommendations, to remove unrealistic values, to verify the assumptions for the Eddy Correlation method and to ensure the data quality (Beziat et al., 2009). In the following, we referred to the wind speed and the Bowen ratio available among these onsite measurements.

3 Theoretical analysis of absorption effects on the signal of an LAS

In this section, we describe and analyze some theory that underlies the measurement of the structure parameter for the refractive index of air C_{n^2} based on scintillometry. Two main effects contribute to the estimation of C_{n^2}. Absorption is due to large-scale eddies, and it affects the low-frequency part of the power density spectrum. Meanwhile, refraction is introduced by eddies of the size of the beam diameter.

3.1 The relationship between the structure parameter and the scintillometer signal in the absence of absorption

The structure parameter of the refractive index of air, C_{n^2}, characterises the atmospheric turbulence using the spatial correlation of the refractive index of air, *n*. In the case of homogeneous and isotropic turbulences, C_{n^2} is expressed as:

$$C_{n^2} = \frac{\overline{[n(x+r)-n(x)]}^2}{r^{\frac{2}{3}}} \tag{1}$$

where $l_0 << r << L_0$, x is the spatial position located in 3D coordinates, r is the distance between two measurement points, l_0 is the inner scale of turbulence, and L_0 is the outer scale of turbulence. These two scales define the inertial subrange of turbulences; L_0 corresponds to the transition with eddy production (*i.e.*, the largest eddies), and l_0 corresponds to the transition with dissipative subranges (*i.e.*, the smallest eddies).

A scintillometer is composed of a transmitter that emits an electromagnetic beam and a receiver that focuses this radiation and measures signal fluctuations caused by the atmosphere. Based on measurements of the logarithm of the intensity fluctuations of an electromagnetic wave propagating through the atmosphere, the scintillometer can estimate C_{n^2} integrated along its transect. The relation between the scintillometer measurement and C_{n^2} is, in the case of a large aperture instrument (Appendix A, Eq. 8):

$$C_{n^2} = 4.48 D^{7/3} L^{-3} \sigma^2_{\ln I} \tag{2}$$

where $D >> \sqrt{\lambda L}$, D is the aperture diameter of the beam, L is the path length, λ is the wavelength of the propagating beam, and σ^2_{lnI} is the variance of the logarithm of the signal (*i.e.*, intensity fluctuations).

However, the C_{n^2} derived from the scintillometer measurement (Eq. 2) can differ from the C_{n^2} described by Eq. 1. Firstly, Eq. 1 provides an instantaneous value of the C_{n^2} whereas the receiver sensor integrates the C_{n^2} value, estimated with Eq. 2. Besides, some assumptions are required to derive the structure parameter of the refractive index of air with Eq. 2. For instance, the atmosphere is supposed to be an absorption free medium, and the turbulences that cause the signal fluctuations recorded by the receiver are assumed to be in the inertial subrange only. With this set of hypotheses, we can assimilate the C_{n^2} measured with the scintillometer (*i.e.* derived from Eq. 2) to the real definition of C_{n^2} (*i.e.* from Eq. 1).

3.2 The theoretical contribution of absorption to the C_{n^2} measured with an LAS and parameters influencing absorption

As explained in the section above, Eq. 2 is exact only if the atmosphere is considered as a transparent medium; that is, the refractive index is assumed to be a real number. In practice, this is not the case in the atmosphere, as the transmitted signal is attenuated due to molecular absorption lines and nebulosity. For instance, for the near-infrared range around 940 nm, the absorption lines of the atmosphere are displayed in Figure 1. This absorption is mainly due to water vapour; in this case, attenuation is higher for a longer transect.

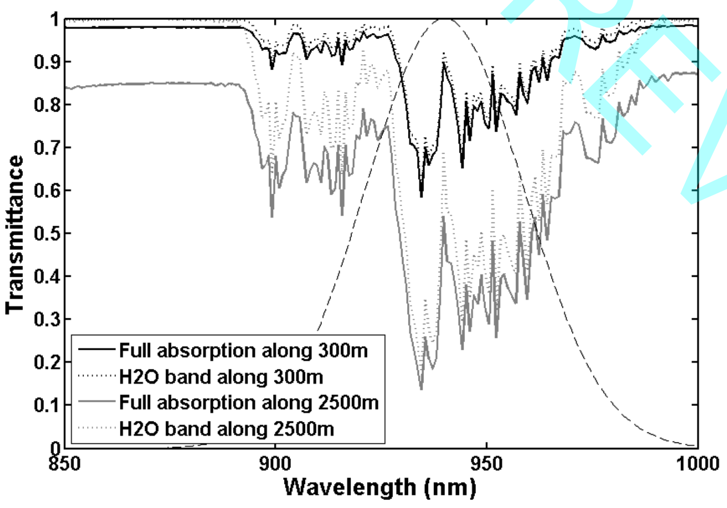

Figure 1 Transmittance of the atmosphere around 940 nm calculated using MODTRAN and, considering only the water vapour absorption (dotted line) and all attenuations (solid line) for L = 300 m, HR = 50%, T = 293 K (in black) and for L = 2500 m, HR = 50%, T = 293 K (in grey). The emission diagram of the LED is also displayed (grey dashed line).

To evaluate the effects of both refraction and absorption on the measurement, the refractive index of air must be considered a complex number. Its real part, n_R, is indeed representative of the refractive phenomena, while the imaginary part, n_I corresponds to absorption. As such, the variance of the log amplitude fluctuations in conditions of high humidity can be expressed as (Hill et al. 1980):

$$\sigma^2_{\ln A} = \sigma^2_R + \sigma^2_I + \sigma_{IR} \quad (3)$$

where σ^2_R is the variance due to refractive phenomena, σ^2_I is the variance due to absorption phenomena, and σ_{IR} is the covariance between refraction and absorption phenomena. Each term in Eq. 3 is expressed by decomposition of the structure parameter into parts corresponding to real and imaginary phenomena. Thus, C_{nR^2} is the structure parameter of the real part of n, C_{nI^2} is the structure parameter of the imaginary part of n, and C_{nIR} is the cross-structure parameter between the imaginary and real parts of n, Eq. (4).

$$C_{nIR} = \frac{\overline{[n_I(x+r) - n_I(x)][n_R(x+r) - n_R(x)]}}{r^{\frac{2}{3}}} \quad (4)$$

Hill et al. (1980) studied the impact of σ^2_I and σ_{IR} versus σ^2_R at the wavelengths of 12 µm and 25 µm; *i.e.*, the authors tried to quantify the effects of both refraction and absorption. However, at the wavelength that we used (940 nm), no previous study was available, so we had to determine the contribution of each phenomenon (presented in Annexe 1). A theoretical study at this wavelength is indeed a necessary prerequisite for the experimental determination of the absorption contribution.

To identify the conditions for which we expect a high contribution of absorption to the measurement, we had to perform a sensitivity analysis of each variance component, *ie.* an estimation of the relative weight of each variance component. The computation of each variance component (σ^2_R, σ^2_I, σ_{IR}) when using a complex refractive index, is fully explained in Appendix A.

Actually, the ratio $(\sigma_{IR}+\sigma^2_I)/\sigma^2_R$ is mainly controled by the Bowen ratio value and the shape of turbulent spectrum (see appendix A). To compute the variances, we assume that turbulences can be described by an idealized energy spectrum like the Kaimal spectrum (Foken, 2008, Kaimal et al., 1972). Using such a spectrum is better adapted to our study than a Kolmogorov spectrum (limited to the inertial subrange), as it is defined for low wavenumbers. The shape of the energy turbulent spectrum has been parametrized from the energy q-spectrum calculated from the turbulent dataset (EC measurements). This latter is proportionnal to $(1+12.5z_mK)^{-5/3}$, where K, is the spatial wavenumber, and z_m, the measurement height.

We considered two wind speed values (0.5 and 5 m.s^{-1}) and the impact of the Bowen ratio (using the turbulent dataset) to estimate the sensitivity of $(\sigma_{IR}+\sigma^2_I)/\sigma^2_R$ to low wavenumbers. Values of |β| lower than 0.1 were rejected in agreement with the correlation assumptions between T and q (see Appendix A). The results of $(\sigma_{IR}+\sigma^2_I)/\sigma^2_R$ versus β are plotted in Figure 2, at two wind speed values (0.5 and 5 m.s^{-1}). As |β| decreases, the ratio $(\sigma_{IR}+\sigma^2_I)/\sigma^2_R$ increases. However, this behaviour strengthens as the wind speed increases. Maximum values of $(\sigma_{IR}+\sigma^2_I)/\sigma^2_R$ increase fom 2% to 26 % when wind speed increases from 0.5 and 5 m.s^{-1}. A similar study has been realized considering a Kolmogorov spectrum for turbulences behaviour, hence, reducing the turbulent spectrum to its inertial subrange. The resulting $(\sigma_{IR}+\sigma^2_I)/\sigma^2_{R}$ does not exceed 1.5%. Thus large eddies may have a large impact on the contribution of absorption to the C_{n^2} measured by a scintillometer.

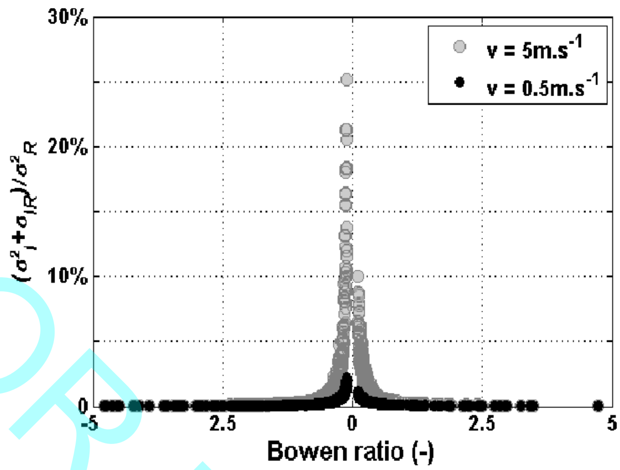

Figure 2 Contribution of absorption $(\sigma_{IR}+\sigma^2_I)/\sigma^2_R$ estimated from theoretical equations versus the Bowen ratio for various wind speeds (0.5 and 5 m s^{-1})

Finally, theoretical results show that absorption mainly influences the value of C_{n^2} under conditions of a very low Bowen ratio, when wind speed is strong. Likewise, the shape of the turbulent spectrum has to be taken into account.

3.3 Determination of the absorption phenomena on the LAS Power Spectrum Density

Absorption and scintillation (*i.e.*, refraction) depend on eddy size. On one hand, absorption is a path-integrated phenomenon introduced by large-scale eddies. On the other hand, the scintillation effect measured by an LAS is due to eddies that have a similar size to the beam diameter. As the importance of both phenomena depends on the frequency range, spectral analysis is usually used to separate the two phenomena.

To monitor the absorption phenomenon with an LAS, we analysed the power spectral density of the signal that was recorded on the output of the detector.

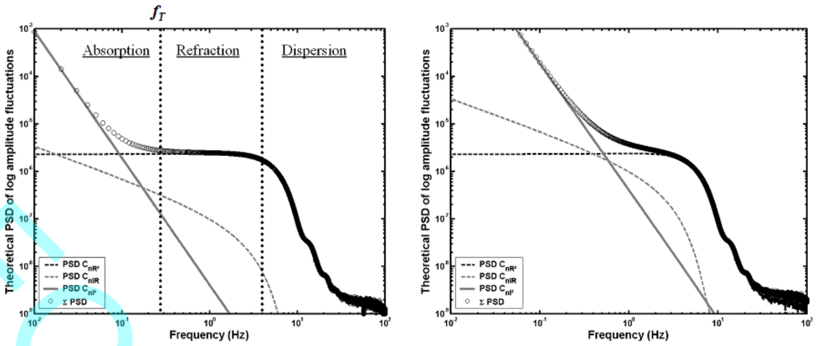

Figure 3 Theoretical power spectrum density (PSD) of the log amplitude fluctuations in dry (left side) and wet (right side) conditions, with D = 15 cm, L = 300 m, v = 1 m s^{-1}, λ = 940 nm and C_{nR^2} = 2.63 10^{-14} m$^{-2/3}$. In dry conditions, C_{nIR} = 4.94 10^{-19} m$^{-2/3}$ and C_{nI^2} = 9.27 10^{-24} m$^{-2/3}$. In wet conditions, C_{nIR} = 4.94 10^{-18} m$^{-2/3}$ and C_{nI^2} = 9.27 10^{-22} m$^{-2/3}$. Contributions of the real and imaginary parts are plotted as PSD C_{nR^2} for the real part and PSD C_{nIR} + PSD C_{nI^2} for the absorption contribution. The transition frequency (f_T) between absorption and refraction is presented in the left side panel.

Three main zones can be identified on the power spectrum (Fig. 3): a low-frequency zone corresponding to absorption, a refraction plateau independent of frequency, and a high-frequency roll off due to dispersion and related to aperture damping. Nieveen et al. (1998) provided analytical expressions of the absorption and refractive plateau of the power spectrum (after correction, Kohsiek 2007, pers. communication):

$$PSD_R = 0.266 L^3 D^{-\frac{4}{3}} C_{nR^2} v^{-1} \qquad (5)$$

$$PSD_I(f) = 0.0326 k^2 L C_{nI^2} v^{5/3} f^{-8/3} \qquad (6)$$

where v is the wind speed perpendicular to the transect (m s^{-1}), k is the wave number (m^{-1}), f is the frequency (Hz), $C_{nR}{}^2$ is the structure parameter of the real part of the air refractive index, and $C_{nI}{}^2$ is the structure parameter of the imaginary part. However, this decomposition is not complete, as it is necessary to introduce the cross-structure parameter between the real and imaginary parts of n, that is, C_{nIR}. Numerical calculations of the density power spectrum of this latter value PSD_{IR} lead to the asymptotic equation:

$$PSD_{IR}\left(f\right)=0.5211L^2kC_{nIR}v^{-1/3}f^{-2/3} \qquad (7)$$

Analytical expressions for the spectra are listed in Appendix B. Thus, this last term can change the expression of the transition frequency (*i.e.*, the transition between absorption and refraction) given by Nieveen et al. (1998). No other analytical expressions can be found for this transition frequency, and therefore, numerical calculation is necessary.

3.4 Understanding the impact of absorption on the accuracy of C_{n^2} using an example

By computing C_{n^2} from the spectrum of scintillation, one can select the refractive effects on the spectrum with quite high precision, excluding any contribution from absorption. For instance, we calculated the power spectrum density of the log amplitude fluctuations on July 17th 2008 at 12 a.m. (Fig. 4a) and 6 p.m. UTC (Fig. 4b). As the raw spectrum of scintillations is noisy, we first processed the data with a logarithmic running mean method in order to smooth the spectrum. We also calculated the expected C_{n^2} assuming no absorption conditions (grey dashed line) according to Eq. 5 and the wind speed measured by a sonic anemometer. We noticed that when scintillation is strong and absorption is weak, as it is the case at midday, the absorption slope is only visible at very low frequencies (Figure 4a). In these conditions, the expected and experimental values of the C_{n^2} are similar (2.9e^{-13} m$^{-2/3}$ compared to 3.07e^{-13} m$^{-2/3}$). Differences between both C_{n^2} are partly due to the accuracy on the the refraction plateau value, and on the wind speed measurement. However, when absorption is stronger but scintillation is weaker, the absorption slope extends up to higher frequencies (Figure 4b). This leads to an expected C_{n^2} (grey dashed line), which is lower than the experimental one, (*i.e.* 2.3e^{-15} m$^{-2/3}$ compared to 1.22e^{-14} m$^{-2/3}$). This is due to an overestimation of the experimental C_{n^2} caused by extra variance integrated in frequencies below 1Hz. Indeed, when the scintillometer measures turbulence, it takes into account the absorption slope and then tends to overestimate C_{n^2}. This highlights the need to filter absorption phenomena to improve the accuracy of C_{n^2} measured by an LAS.

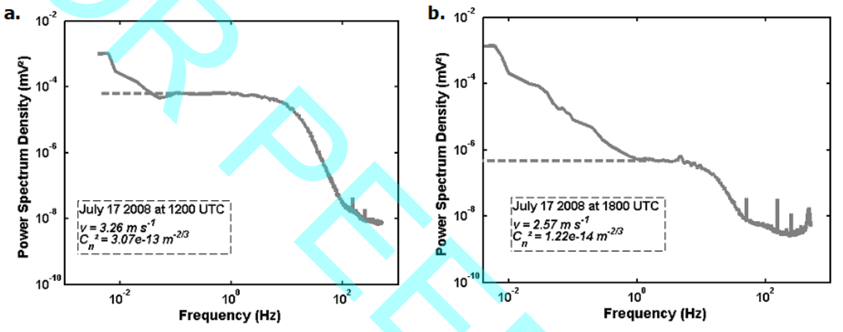

Figure 4 Power spectrum density of log amplitude fluctuations of the signal acquired from the LAS output on July 17 2008 at 1200 UTC (a.) and 1800 UTC (b.). The dashed line corresponds to the PSD_R according to Eq. 19.

3.5 Effect of the wind speed on the LAS Power Spectrum Density

From the previous considerations, it seems important to attenuate the absorption effect on the LAS signal, using an accurate filtering. According to previous theoretical results (section 3.2), the absorption contribution is wind speed dependent, since large eddies may have an important contribution for strong wind speeds. However, even when absorption contribution is negligeable, the wind speed modifies the shape of the power spectrum density (PSD) of the signal of a scintillometer (see appendix B, Eq. 19). In this section, we will focus on the influence of wind speed on the shape of the power spectral density of the signal recorded by an LAS, and on its impact on the choice of the filter.

Results of section 3.2 have shown the impact of wind speed on the shape of the turbulent spectrum at low wavenumbers *i.e.* on the absorption fluctuations contribution. However, the wind speed also affects the high wavenumbers, since it controls the spectral width of the refraction plateau, as shown in Figure 5 (Irvine et al. 2002; Nieveen et al. 1998). High wind speeds increase its spectral width, whereas low wind speeds tend to reduce it. In an ideal case, filtering results must be independent of the wind speed. A theoretical power spectrum density, assuming an absorption-free atmosphere, has been calculated according to Eq. 19 (see Appendix B). Results for similar conditions except different wind speeds (*i.e.* v = 1 and 5 m s^{-1}) are plotted on Fig. 5. Besides, we also computed the Kaimal and Kolmogorov turbulent spectra ~~have been tested for~~ with numerical calculations of the theoretical PSD of the LAS signal ~~of an LAS,~~. But ~~but~~ both spectra lead to the same results~~s~~.

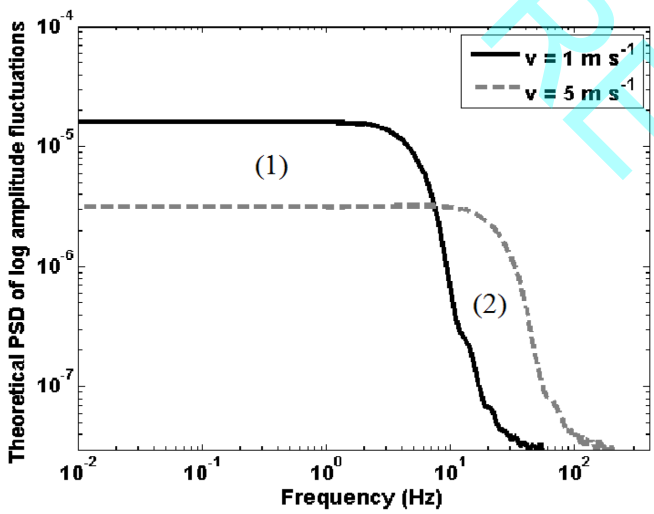

Figure 5 Theoretical power spectrum density of the log amplitude fluctuations of the signal acquired at the output of an LAS for various wind speed : 1 m s^{-1} (black line) 5 m s^{-1} (grey dashed line), according to Eq. 19 of Appendix B. All other parameters are the same : C_{n^2} = 2.63e-14 $m^{-2/3}$, D = 15 cm, L = 565 m and λ = 940 nm.

The signal variance in each case corresponds to the area under the curve. After computation, it appears on Fig. 5 that the area (1) is equal to the area (2). Thus, when filtering the low frequencies with a simple high-pass filter, this will reduce the area in (1) with no modification in (2): it means that we will have a lower variance calculated in low wind speed conditions than in higher ones. So, a part of variance is removed when filtering for low wind speed. This effect will be quantified in the Results and Discussion sections.

4 Description of filtering methodology applied on the LAS signal

4.1 Attenuation of absorption by numerical filtering

The perfect filter for scintillometers should attenuate only the absorption contribution to maintain a homogeneous refractive plateau. In other words, it must properly detect the transition between the low-frequency absorption slope and the refractive plateau. This is rather difficult to perform and achieve using a scintillometer, partly due to the difficulty of data acquisition, spotting the absorption slope and real-time processing. Thus, the standard LAS instrument only uses analogical filtering; this technique is easy to implement, but it lacks accuracy. Here, the configuration we used, *i.e.*, data acquisition and numerical filtering, is likely to accurately reduce the contribution of absorption phenomena to the measurement.

Mis en forme : Police :Times New Roman

Mis en forme : Justifié, Interligne : Double

Mis en forme : Police :12 pt

Mis en forme : Interligne : 1.5 ligne

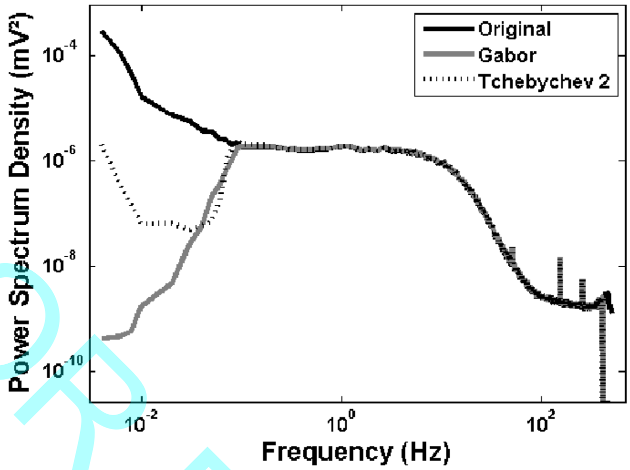

Figure 6 Power Spectrum Density of the signal acquired from the LAS output on July 17 2008 1800 UTC. The original signal (solid black) corresponds to the signal with no filtering, the Gabor signal (solid grey) is the original signal filtered by Gabor filtering BP 0.1-400 Hz, and Tchebychev (dotted black), is the original signal filtered by a Tchebychev 2 filter BP 0.1-400 Hz of order 12.

Various types of numerical filters can achieve this type of filtering. Here, we chose to use a Gabor transform filter. Gabor filtering consists of processing a fast Fourier transform of the signal, which is windowed by a Gaussian function, and then time-scale shifted. The frequency coefficients related to frequencies that must be attenuated are set to 0. Then the Gabor expansion uses these new coefficients to reconstruct the filtered signal (Qian and Chen 1993). Finally, this filter presents good characteristics, as the fall-off is almost vertical, with attenuation close to 40 dB and a fast computation time, which can make it usable for real-time processing. Figure 6 displays the results of signal band-pass filtering (BP) with the Gabor filter as well as with an IIR Tchebychev 2 filter of order 12. In comparison to the Tchebychev technique, the Gabor filter is more efficient and the absorption contribution is completely removed.

Commentaire [a1]: TU la laisses out u l'enlèves cette figure? Si tu l'enlèves, il faut le supprimer dans le texte et dans la liste des légendes.

Mis en forme : Justifié

4.2 Methodology for signal processing

As explained in section 2, the signal at the output of the detector of the scintillometer was recorded at a 1 kHz sampling frequency (hereafter raw signal). Then the raw signal was processed as follows.

a) The logarithm of the signal was calculated.
b) The Gabor transform was applied with a chosen band pass.
c) All Gabor coefficients outside the band pass were set to 0.
d) The signal was recomposed by Gabor expansion.
e) The variance of the signal and hence C_{n^2} were calculated (Eq. 2).

C_{n^2} values are calculated with a 2.5 seconds variance, and then they are averaged over 30-minute periods. The output 'Demod' and 'C_{n^2}' signals were recorded at the same time on a data-logger CR510 (Campbell). To ensure the quality of the data, all periods in which |'Demod'| is under a certain threshold, *e.g.*, 50 mV (Kleissl et al. 2008). However, in our case, 100 mV is more appropriate.

As the aim of our study is to evaluate different kinds of filtering, various Gabor filters (fixed band-pass filters or adaptive ones) were applied and tested on the scintillometer dataset. For instance, commercial LAS uses specific band-pass filters: BP 0.1—-400 Hz or the WUR LAS (Moene et al. 2005), and BP 0.2—-400Hz for –the Kipp&Zonen one LAS (Kleissl et al. 2008). These band pass filters were then tested on our dataset as well as a BP 0.5——400 Hz filter, suggested by Nieveen et al., 1998. The performance of an adaptive filtering will also be analysed.

Besides, a reference value is needed in order to evaluate the performance of each filter. Among the possibilities of deriving a C_{n^2} close to an ideal one, we choose to modify the raw signal so that its power density spectrum is close to PSD_R (Figure 7). Thus,, so that only absorption fluctuations are removed. Indeed, the process is the same as described above, except that the low cut-off frequency varies to fit the transition frequency. The transition frequency, hereafter f_T, represents the frequency at which the absorption slope intercepts the refractive plateau, *i.e.*, the transition frequency between absorption and refractive areas (see Figure 3). Then, the Gabor coefficients outside the band pass (step c) are not set to 0, but their value is kept at the value of the refractive plateau. Thus, we have achieved a reconstructed spectrum, which is representative of a *reconstructed* C_{n^2} (Figure 7). This *reconstructed* C_{n^2} is considered as a reference in the "results section, as ~~is~~ it is supposed to be an 'ideal' C_{n^2} *i.e.* not affected by absorption fluctuations.

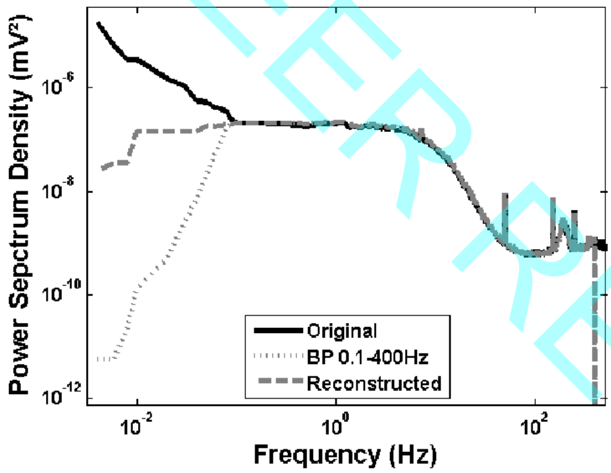

Figure 7 Power Spectrum Density of the signal acquired from the LAS output on July 17 2008 800 UTC. The original signal (solid black) corresponds to the signal with no filtering, BP 0.1-400 Hz (dotted grey) is the original signal filtered by Gabor filtering BP 0.1-400 Hz, and Reconstructed (dashed grey) is the original signal filtered by Gabor filtering BP f_T-400 Hz, but where the coefficients outside the band pass are set to the refractive plateau value.

Hereafter the C_{n^2} derived from these different filtering ~~processes~~ will be denoted as :

- C_{n^2} -*(reconstructed)* is another way of notingor *reconstructed* C_{n^2} . It is the reference measurement of this paper. It is an ideal value without absorption phenomenon.er.
- C_{n^2} *(raw signal)* corresponds to the raw signal where only frequencies above 400Hz are attenuated.
- C_{n^2} –*(fixed band pass)* corresponds to the raw signal filtered by a fixed band pass filter. Three types of fixed band pass filters are discussed in this paper: BP 0.1 - 400Hz, BP 0.2 - 400Hz and BP 0.5 - 400Hz
- C_{n^2} –*(adaptive band pass)* corresponds to the raw signal filtered by an adaptive band pass filter, *e.g.* BP f_T - 400Hz

5 Results

Gabor filtering was applied to optimise the band-pass filter of the LAS and then to quantify the contribution of absorption to the C_{n^2} measurements, on a 12-day dataset between August 2 and August 13 2008. A preliminary study has been realized to evaluate the performance of Gabor filtering. Then, optimisation was performed by considering traditional filtering with a fixed cut-off frequency. For a given low cut-off frequency, the observed variance depends on the upper corner frequency (and therefore on the width of the refractive plateau), which varies linearly with wind speed (Nieveen et al. 1998). Therefore, the frequency response of the filter must be chosen so that the variations of the C_{n^2} upon the width of the refractive plateau are negligeable. Then, to estimate the contribution of absorption to the C_{n^2} measurement, we applied an adaptive filtering to the signal from the LAS output.

5.1 Evaluation of Gabor filtering on the raw signal : comparison with the C_{n^2} measured by an LAS

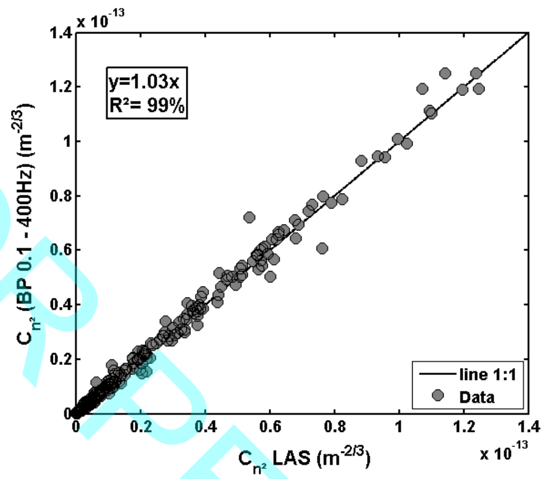

Figure 8 Comparison between C_{n^2} *LAS* from the LAS output 'C_{n^2}' and C_{n^2} calculated from the raw signal filtered by a Gabor filtering BP 0.1-400 Hz.

First, to evaluate the accuracy of Gabor filtering, we compared values of C_{n^2}, derived from the raw signal, to which a Gabor filter has been applied, with C_{n^2} LAS, calculated by the WUR LAS. Indeed, we implemented the same filtering as the one of the electronics of the WUR LAS, which is a band pass filter ~~BP~~ 0.1–-400-Hz. The results are displayed in Figure 8. They show an excellent correlation (R^2=99%) and a regression slope close to unity. The slight difference in the slope is probably due to the electronics or to the calibration of the transect length. This latter kind of error can approach 6% of the value of C_{n^2} (Moene et al. 2005).

Thus, this first experimental step shows that our acquisition and processing system can be used to test and evaluate other kinds of filtering.

5.2 Estimation of the contribution of absorption to the C_{n^2} measured by an LAS

The C_{n^2} measured by an LAS can be overestimated by the contribution of absorption. As it has been previously described, spectral analysis is the only way to differentiate the absorption contribution from the refraction (scintillation). By comparing the C_{n^2} (raw signal) and the "reconstructed C_{n^2}", we aim at quantifying the absorption contribution on the C_{n^2} measured by the LAS. The first step is then to detect f_T in order to create the reconstructed signal.

There is no automatic tracking available to perform f_T detection accurately, so detection must be supervised by an operator. We computed the power spectra over 5 minutes, which correspond to the largest time interval affordable with respect to computation constraints. Then, we determined the transition frequency for each spectrum for the 12-day dataset from August 2 to 13 2008. Transition frequencies are plotted on Fig. 9 with the demodulated signal. The average frequency detected on this dataset is estimated at 0.1Hz but is highly variable, with a maximum value at 1.5Hz.

The "reconstructed Cn^2", described in section 4.3, has ~~then~~ been calculated using the transition frequencies. The C_{n^2} (raw signal) has been compared to the "reconstructed C_{n^2}". Then, it is possible to quantify the effect of absorption contribution on the signal recorded by a scintillometer, hereafter denoted as the relative difference ΔC_{n^2} = [C_{n^2} (*raw*) - C_{n^2} (*reconstructed*)]/ C_{n^2} (*reconstructed*). The average contribution of absorption phenomena is estimated at 1.6% over the period, but it is highly variable with maximum values at 81%.

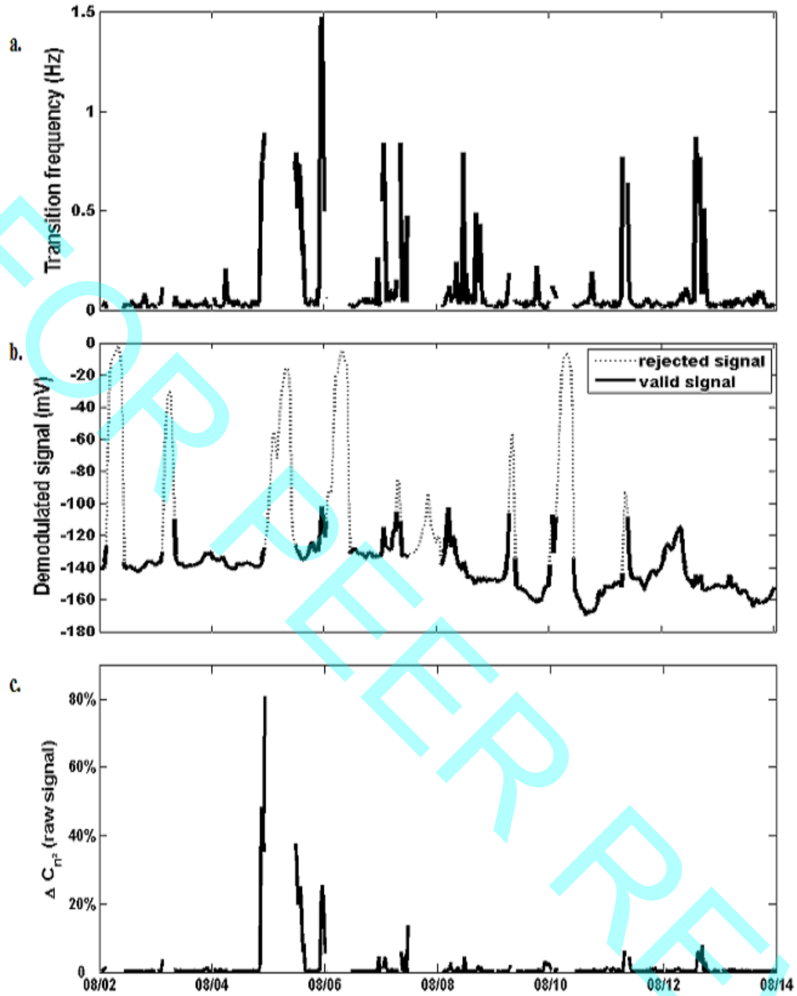

Figure 9 a) Time series of the transition frequency, b) the demodulated signal (values of Demod > -100 mV are in a grey dashed line, and the other values are in a black solid line), c) ΔC_{n^2}= ([C_{n^2} (raw signal) – C_{n^2} (reconstructed)]/ C_{n^2} (reconstructed)) between August 2 and August 13 2008.

These results clearly show that the absorption phenomenon occasionally affects the $C_n{}^2$ estimates ; so there is a real need of applying better filters to the signal of the LAS, in order to improve the accuracy on the C_{n^2}.

5.3 Evaluation of the results of a band pass filtering

5.3.1 The wind speed dependence of the width of the refractive plateau

The lower cut-off frequency of the LAS we used from WUR was set at 0.1 Hz (Moene et al. 2005), whereas for the commercial LAS from Kipp&Zonen, for instance, it is set at 0.2 Hz (Kleissl et al. 2008). Nieveen et al. (1998) even suggested to increase this lower cut-off frequency to 0.5 Hz. These choices represent a compromise between attenuation by absorption phenomena and conservation of refraction effects, although the influence of the wind speed on the refraction plateau is not taken into account. Therefore, we decided to test various filtering effect under various wind speed conditions. Experimental results will be ~~presented in regards~~confronted ~~of~~ to theoretical ones.

The ~~T~~theoretical -power spectrum density, calculated in section 3.5, ~~were~~ is processed to evaluate the underestimation of the variance induced by filtering effect. This underestimation has been estimated for three cut-off frequencies : 0.1, 0.2 and 0.5 Hz, ~~in regards of~~according to different wind speed values. The results are displayed in Table 1. For low wind speed conditions ($v = 0.2$ m s^{-1}), even the lowest cut-off frequency has an influence on the measured variance : we notice a 8.7%. This underestimation increase to 43.6% when filtering below 0.5 Hz. Otherwise, in strong wind speed conditions ($v = 2.5$ m s^{-1}), the maximum variance underestimation does not exceed 3.4%.

Then, we applied Gabor band pass filtering with the same cut-off frequencies (0.1, 0.2 and 0.5 Hz) on the data time series from August 2 to August 13 2008. First, the relative differences were calculated between filtered values of C_{n^2} and the raw signal in the case of very low transition frequencies, i.e f_T << 0.1

Hz. In these conditions, the contribution of absorption can be neglected, and the raw signal is considered to be the same as the reconstructed one.

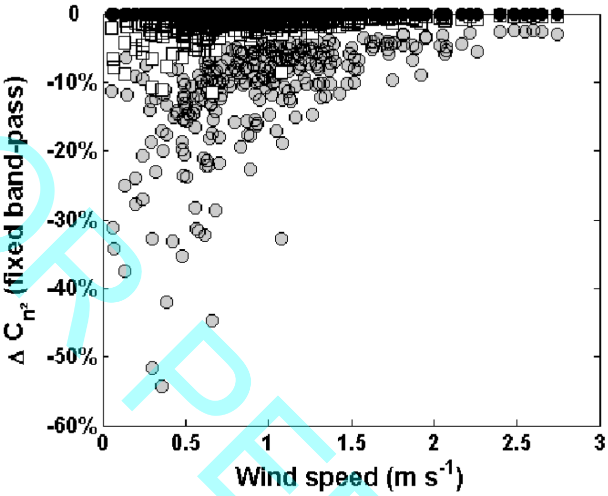

Figure 10 Relative differences ΔC_{n^2}= ([C_{n^2} (fixed band pass) – C_{n^2} (reconstructed)]/ C_{n^2} (reconstructed)) are plotted as a function of wind speed for various filters, in condition of negligeable absorption contibution. The various band-pass filters studied here are BP 0.1- 400 Hz (black circles), BP 0.2 - 400 Hz (white squares), and BP 0.5 - 400 Hz (grey circles).

According to Figure 10, we observe low ΔC_{n^2} versus wind speed in the case of the BP 0.1-400 Hz; this means that the effect of filtering between 0.1 and 400 Hz is nearly constant with wind and does not influence relative differences in C_{n^2}. The maximum ΔC_{n^2} value obtained in this case is estimated at 0.5% for v = 0.2 m s^{-1}. Therefore, in these conditions, the variance of the signal (and hence C_{n^2}) is not dependent on the width of the refractive plateau. In contrast, the BP filter 0.5-400 Hz has a stronger effect under low wind speeds than under wind speeds greater than 1.5 m s^{-1}. Actually, ΔC_{n^2} values can raise up to 55% (v < 0.4 m s^{-1})-, and are always greater than 2 %. These results are in good accordance with expected ones shown in Table 1. –Thus, we can conclude that a portion of the variance is omitted when computing C_{n^2} with a fixed band-pass filter, as C_{n^2} depends on the width of the refractive plateau. The BP filter 0.2-400 Hz is also rather independent of wind speed, however, ΔC_{n^2} values can reach up to 12 % under low wind speed conditions.

This preliminary study aims to support choice of WUR and Kipp&Zonen with respect to the band-pass filtering used in their scintillometers. Thus, we can exclude the BP 0.5-400 Hz filter, as it triggers a residual underestimation of the C_{n^2} by 2 %. However, to this end, we still cannot make conclusions regarding the efficiency of these filters when accurately filtering absorption.

4.3.2 Effectiveness of a band pass filtering

The results of both remaining filters (BP 0.1~~—~~-400 Hz, and BP 0.2~~—~~-400 Hz) have been compared with the ‘reconstructed’ signal on the whole data set, to highlight their effectiveness to remove absorption. The ~~R~~results of the ΔC_{n^2} = [C_{n^2} (*fixed band-pass*) - C_{n^2} (*reconstructed*)]/ C_{n^2} (*reconstructed*) versus wind speed have been plotted on Fig.11. The impact of both filters when applied in absorption-free conditions leads to an underestimation of C_{n^2}, whereas in absorption conditions, the filters introduce an overestimation of C_{n^2}. According to Figure 11, the average contribution of the absorption phenomena (which cannot be separated from the wind speed sensitivity) to C_{n^2} is estimated at 0.7% (± 5%) or 0.6% (± 5%), for respectively a 0.1 Hz or 0.2 Hz low cut-off frequency. However, some spectra are more affected by absorption, with values of ΔC_{n^2} rising up to 70% for the BP 0.1-400Hz filter (respectively 60% for the BP 0.2-400Hz filter).

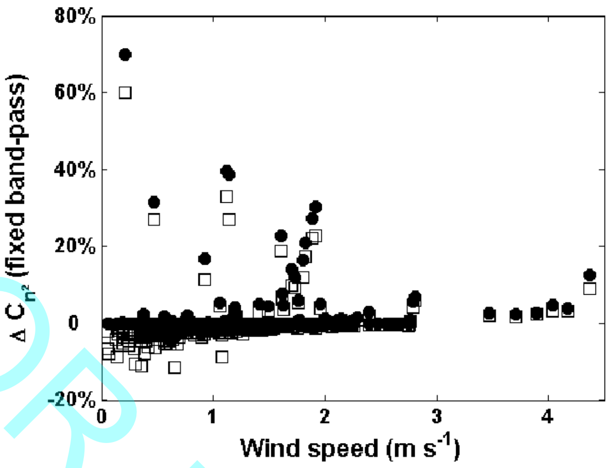

Figure 11 Relative differences ΔC_{n^2}= ([C_{n^2} (fixed band pass) – C_{n^2} (reconstructed)]/ C_{n^2} (reconstructed)) are plotted as a function of wind speed for 2 BP filters, between August 2 and 13 2008. The various band-pass filters studied here are BP 0.1- 400 Hz (black circles) and BP 0.2 - 400 Hz (white squares).

Thus, the final choice of the low cut-off frequency is dependent on experimental conditions. The BP filter 0.2-400 Hz is preferable when using scintillometers in windy regions (wind speed > 0.5 m s^{-1}), as the absorption contribution is reduced and the filtering is nearly independent on wind conditions. The BP filter 0.1-400 Hz is preferable in others cases as the effectiveness of the filtering is nearly not affected by wind conditions.

5.3 Improvements due to the use of an adaptive filtering

Instead of using a fixed low cut-off frequency value for a band-pass filter, we can complete and improve previous results with an adaptive filter (*i.e.*, band-pass filtering) of the type f_T-400 Hz, where f_T is the transition frequency between absorption and refraction, described in sections 3.3 and 4.1. In this way, we can take advantage of filtering with little sensitivity to wind speed, and by attenuating all absorption contribution.

Then, we applied the Gabor transform to the dataset and performed an expansion with these adaptive frequencies, according to the Gabor filtering description in section 4.1. We compared the relative differences between the results of ‘adaptive filtering’ and ‘reconstructed’ C_{n^2} (Figure 11c). These relative differences are computed as before according to the expression: ΔC_{n^2} =[C_{n^2} (*adaptive filtering*) - C_{n^2} (*reconstructed*)]/ C_{n^2} (*reconstructed*). To remain coherent with previous results, we display the results of ΔC_{n^2} -versus the wind speed. The same dataset is considered, and ΔC_{n^2} is plotted in black circles in figure 12. The effectiveness of the filtering of the signal from the LAS output is improved as the averaged ΔC_{n^2} is around -0.06% whatever the wind speed. In this case, C_{n^2} is always underestimated but ΔC_{n^2} does not exceed –3% in the worst cases.

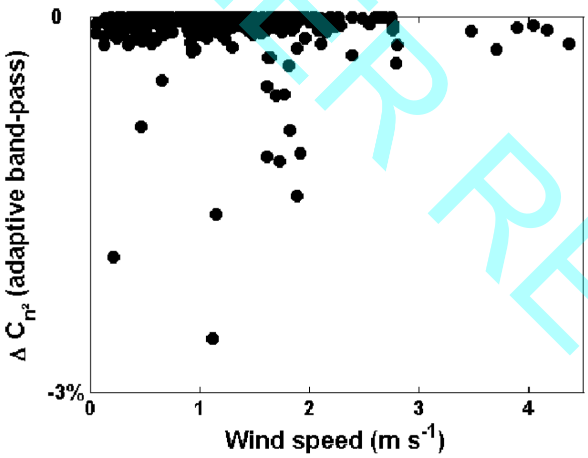

Figure 12 Relative differences ΔC_{n^2} = ([C_{n^2} (adaptive band-pass) – C_{n^2} (reconstructed)]/ C_{n^2} (reconstructed)) are plotted as a function of wind speed for an adaptive band pass filtering, between August 2 and 13 2008.

Finally, the use of an adaptive filtering could be the solution to 1) attenuate absorption and 2) reduce the sensitivity of the filter to wind speed conditions.

6 Discussion

In the previous section, we presented promising results on the filtering of the LAS signal in agreement with its sensitivity to wind speed and the absorption fluctuations attenuation. Indeed, we manage to highlight these various effects on an experimental dataset and to quantify it. However, these results have to be discussed regarding to theoretical results.

For instance, when studying the effect of the wind speed, we showed that the underestimation of the variance due to a fixed band-pass filtering is in good agreement with the results obtained in Table 1 (see section 4.3). A slight underestimation of the experimental results compared to theory can be noticed, mainly for low cut-off frequencies. This can be explained by the lack of accuracy of filtering when the cut-off frequency decreases. On the contrary, the theory did not forecast the large spread, observed in the results of Fig. 10 at low wind speeds. The theoretical calculations have been performed using two turbulent spectral shapes (see section 2.5): one proposed by Kolmogorov (1941) that only considers the refractive phenomenon (scintillation) in the inertial subrange, and the other proposed by Kaimal et al. (1972) corresponding to an ideal case. The comparison of the 2 turbulent spectra gives similar results. Then, the large spread observed in the results of Fig. 10 can-not be explained by the shape of the turbulent spectrum. Another hypothesis that seems to be more consistent is the difference between the local measurement of the wind speed by the sonic anemometer and~~,~~ the wind speed variations along the path of the scintillometer. However, there is no measurement of the integrated wind speed along the scintillometer path so in Fig. 11, the wind speed value is a local one measured with the sonic anemometer. ~~However, no measurements are available to verify this hypothesis.~~

TheE experimental results of section 5.2 on the contribution of absorption to the C_{n^2} measured by an LAS (section 5.2) differ from expected ones (section 2.2). Actually, by definition, ΔC_{n^2} (raw signal) should be the same as $(\sigma_{IR}+\sigma^2_{I})/\sigma^2_{R}$. However, theoretical values of $(\sigma_{IR}+\sigma^2_{I})/\sigma^2_{R}$, calculated with our turbulent dataset do not exceed 1.2% for a Kolmogorov spectrum, whereas they can reach 23% when considering a Kaimal spectrum. Although experimental results of section 5.2 showed an average value close to the theoretical results (ΔC_{n^2} (raw signal) is close to zero most of the time), there are also events with a strong absorption contribution, which do not correspond to theoretical calculations since ΔC_{n^2} can reach 80%. Moreoever, in these latter cases, neither the wind speed nor the Bowen ratio, can be related to the presence of strong absorption contribution. Therefore, we focussed on the behaviour of the turbulent spectrum using turbulent values of temperature (*T*) and humidity (*q*), recorded at 20Hz with the flux tower instruments. August 5 was chosen for the comparison, as the maximum transition frequencies (1.47 Hz) were observed on this day. Three periods have been compared, the first one at 730 UTC (Figure 14 a. & d.) close to the transition between stable and unstable atmospheric regimes, the second one, at 1400 UTC (Fig. 14 b & e) when turbulence is developped, and the last one at 2000 UTC (Fig. 14 c & f) during stable conditions. Results at 730 UTC (Fig. 14a) show a large discrepancy between *q* and *T* spectrum, due to the contribution of energetic low frequencies phenomena in the *q*-spectrum. This behaviour is translated into the power density spectrum of the raw signal of the scintillometer, and then induced a large contribution of absorption, about 39% of C_{n^2} (Fig. 14d). At the beginning of the afternoon, at 1400 UTC, both *T* and *q* spectrum spectra have the characteristic shape of the turbulent spectrum suggested by Kaimal et al. (1972) (Figure. 14b). This results in a nearly perfect refractive plateau (no

Mis en forme : Anglais (Royaume-Uni)
Mis en forme : Anglais (Royaume-Uni)
Mis en forme : Anglais (Royaume-Uni)
Mis en forme : Anglais (Royaume-Uni)
Mis en forme : Anglais (Royaume-Uni)
Mis en forme : Anglais (Royaume-Uni)
Mis en forme : Anglais (Royaume-Uni)
Mis en forme : Anglais (Royaume-Uni)
Mis en forme : Anglais (Royaume-Uni)
Mis en forme : Anglais (Royaume-Uni)
Mis en forme : Anglais (Royaume-Uni)
Mis en forme : Anglais (Royaume-Uni)
Mis en forme : Anglais (Royaume-Uni)
Mis en forme : Anglais (Royaume-Uni)
Mis en forme : Anglais (Royaume-Uni)
Mis en forme : Anglais (Royaume-Uni)

absorption contribution) on the power density spectrum of the raw signal of the scintillometer (Figure 14e). Eventually, at 2000 UTC, the humidity (*q*) power spectrum density increases at low wavenumbers, whereas the temperature spectrum is nearly constant (Fig. 14c). Moreover, the wind speed is higher at 2000 UTC and it reaches 2.7 m s^{-1}, whereas the wind speed is 0.2 m.s^{-1} and 0.9 m s^{-1}, at 0730 UTC and 1400 UTC respectively. Therefore, in these conditions, the high transition frequency (1.47 Hz) can be explained by a low refractive plateau (high wind speed and low temperature fluctuations), and a high contribution of low wavenumbers in the humidity spectrum (Figure 14f.). Although the transition frequency is the highest observed in this dataset, ΔC_{n^2} only worth 23%, which is far from its maximum (81%). This may be due to the lack of performance of the filtering in low signal to noise conditions.

Mis en forme : Non Exposant/ Indice

Eventually, these results show the importance of the shape of the turbulent spectrum, and mainly of the *q*-spectrum, on the contribution of absorption on the C_{n^2} measured by an LAS. In most cases, the analysis of the signal of the scintillometer can be performed by only considering the turbulence in the inertial subrange as the results with an idealized spectrum (Kaimal et al., 1972) do not improved our results.

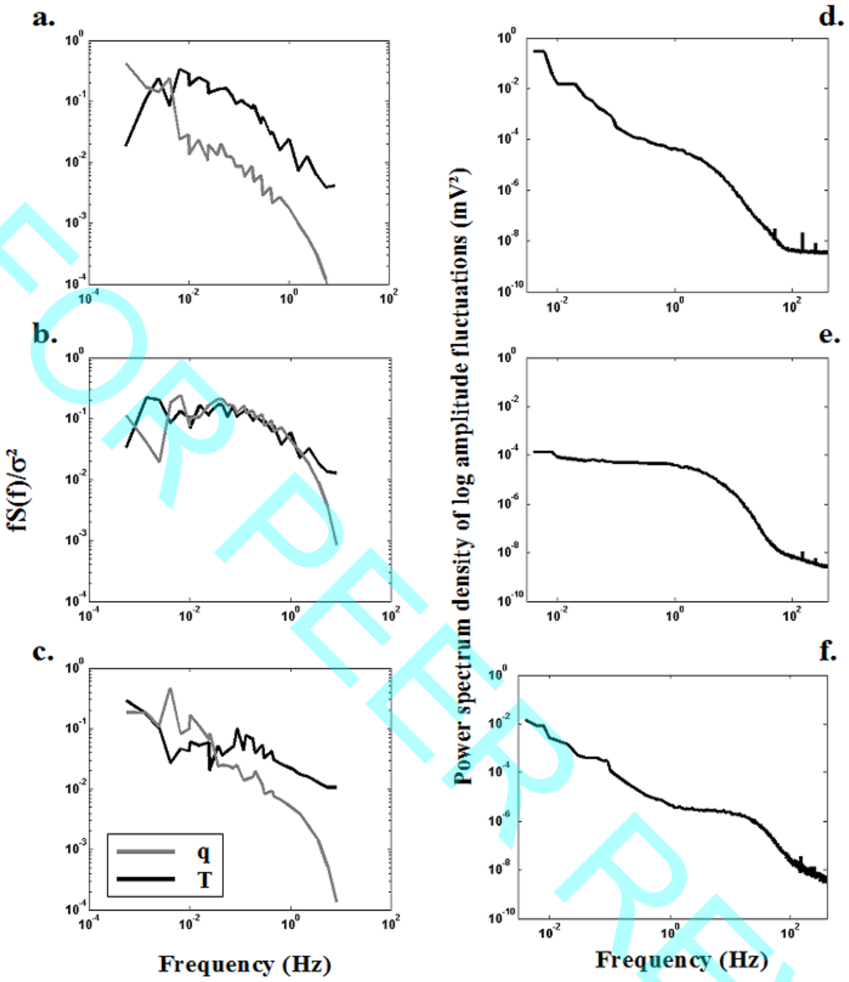

Figure 13 On the left side, normalized energy turbulent spectrum of q (grey lines) and T (black lines). On the right side, power spectrum of log amplitude fluctuations of the signal recorded at the output of an LAS. Three cases are presented here for July 5 : 730 (a. and d.), 1400 (b. and e.) and 2000 (c. and f.) UTC.

6 Conclusion

In this study, raw measurements with an LAS were used to evaluate various type of filtering techniques to understand and quantify the contribution of absorption to the C_{n^2} measurement. Accuracy filtering was performed with the Gabor transform and expansion. This filtering technique offers the opportunity to create filters with various frequency responses with high accuracy and fast computation time.

A first analysis was realized to quantify the contribution of absorption on the raw signal of the scintillometer, using a varying low cut-off frequency. This low cut-off frequency corresponds to a transition frequency between the absorption slope and the refraction plateau. Transition frequencies were detected on 5-minute spectra measured between August 2 and August 13 2008. Using these transition frequencies, we implemented a reconstructive filtering that only removes absorption, and then, the low frequency part of the spectrum was replaced with the refractive plateau. This approach allowed us to estimate the contribution of absorption to the structure coefficient C_{n^2} measured with an LAS, and will be used as a reference. The results show that the averaged contribution of absorption to C_{n^2} values over the entire period of 12 days (averaged over 30 minutes) is only 1.6% (±6%). However, occasionally, this contribution can reach up to 81%. Though the global trend is in agreement with the theory (≈1%), local values tend to be larger. In fact, these cases can be attributed to the presence of energetic eddies at low wavenumbers in the turbulent *q*-spectrum, and are often correlated to an increase of the demodulated signal. These results highlight the importance of the shape of the turbulent spectrum, and mainly the low wavenumbers contribution, to explain absorption contribution on the C_{n^2} measured by an LAS

Different types of filters, based on Gabor filtering methods, have been evaluated in order to accurately remove absorption fluctuations on the C_{n^2} measured by an LAS. Fixed band-pass filters were first studied, as they correspond to common filters on commercial LAS. Then, we studied an adaptive filtering. Each type of filtering was evaluated considering its effect to attenuate absorption and to preserve the refractive plateau, affected by the wind speed. The wind speed is indeed important because it influences the size of the refractive plateau on the scintillation spectrum. This study allowed us to show that band-pass filters BP 0.1-400 Hz and BP 0.2-400 Hz are particularly suitable for the computation of the C_{n^2} because they are independent of the wind speed (0.1 to 3 m s^{-1}). However, none of these filters is able to accurately remove the absorption phenomena. Thus, an adaptive filtering method based on the attenuation of the signal at frequencies lower than the transition frequency has been tested on the raw C_{n^2} data. Results are improved as C_{n^2} values are close to the reconstructed signal, with a maximum underestimation of 3%.

Eventually, the optimal processing to improve the accuracy of the C_{n^2} measured by a scintillometer should be to reconstruct the signal as suggested in this paper. However, this method has to be evaluated with independent measurements of the C_{n^2}. Moreover, these adaptive methods are limited by their ability to derive low cut-off frequencies. In fact, there is no fast and easy solution to automatically and accurately detect the transition frequency. Therefore, using automatic tracking always leads to misdetections that can trigger large discrepancies.

The correction of the measurement of C_{n^2} given by the absorption phenomena is usually addressed in terms of technological issues. However, lacking the necessary technological breakthrough, another approach might be to increase the limitation on the demodulated signal and to ignore C_{n^2} measurements when the variations in 'Demod' are too strong. Another possibility for decreasing the contribution of absorption is to use new devices that rely on two detectors (namely, receivers), either with a correlation function (BLS from Scintec, Kleissl et al. 2009) or two different wavelengths (Solignac 2009b). This latter option consists in comparing the measured C_{n^2} for two near-wavelength signals. One wavelength corresponds to an absorption band, whereas no absorption occurs at the other wavelength. A quantification of the reliability of these methods remains necessary.

APPENDIX A

Calculation of the theoretical variances of the real and imaginary parts of the log amplitude fluctuations for LAS

This appendix describes the expression of the variance of the real and imaginary parts of the log amplitude fluctuations of a beam propagating through a lossy medium. This appendix is based on the work of Hill et al. (1980), which has been adapted to LAS.

For spherical waves propagating on a path length L, consider a light beam of optical wave number k that propagates in a medium that attenuates the light through absorption and refraction phenomena. Hill et al. (1980) expressed the variance of the log amplitude for a large aperture transmitter and receiver as:

$$\sigma_{\ln A} = 4\pi^2 k^2 \int_0^L dz \int_0^\infty dKK \left[\Phi_R \sin^2(\theta) + \Phi_I \cos^2(\theta) + \Phi_{IR} \sin(2\theta) \right] \times \phi_{Airy}$$

$$\text{with } \phi_{Airy} = \left\{ \frac{2J_1(\frac{KDz}{2L})}{\frac{KDz}{2L}} \right\}^2 \left\{ \frac{2J_1(\frac{KD(L-z)}{2L})}{\frac{KD(L-z)}{2L}} \right\}^2 ; \qquad (8)$$

where D is the aperture diameter, $\theta = K^2 z(L-z)/2kL$, K is the spatial wavenumber, and z is the path position. $\Phi_R(K)$, $\Phi_I(K)$ and $\Phi_{IR}(K)$ are respectively the spatial power spectra of the real part, imaginary part and cross-correlation between real and imaginary part of the refractive index. If we consider the case of strong humidity fluctuations, δT has a negligible contribution to n_I, but δT and δq contribute to n_R.

$$\Phi_R(K)=\frac{A_T{}^2}{\langle T\rangle^2}\Phi_T(K)+\frac{A_q{}^2}{\langle q\rangle^2}\Phi_q(K)+2\frac{A_T A_q}{\langle T\rangle\langle q\rangle}\Phi_{Tq}(K) \quad (9)$$

$$\Phi_I(K)=\frac{B_q{}^2}{\langle q\rangle^2}\Phi_q(K) \quad (10)$$

$$\Phi_{IR}(K)=\frac{B_q A_q}{\langle q\rangle^2}\Phi_q(K)+\frac{B_q A_T}{\langle T\rangle\langle q\rangle}\Phi_{Tq}(K) \quad (11)$$

where $\Phi_T(K)$, $\Phi_q(K)$ and $\Phi_{Tq}(K)$ are respectively the spectrum of the temperature and the water vapour concentration and their cospectrum. These can be expressed respectively as the structure parameter of temperature C_{T^2}, humidity C_{q^2} and temperature humidity covariance C_{Tq}, times a general turbulent spectrum for scalar fluctuations $\Phi_s(K)$. By identifying the structure parameter of the real, imaginary, and cross real-imaginary part of the refractive index of air, the two variances and the covariance can be expressed (Lüdi et al. 2005).

$$\sigma^2{}_R=0.132\pi^2k^2\int_0^L dz\int_0^\infty dKK\Phi_s(K)\sin^2(\theta)C_{nR^2}\times\phi_{Airy} \quad (12)$$

$$\sigma^2{}_I=0.132\pi^2k^2\int_0^L dz\int_0^\infty dKK\Phi_s(K)\cos^2(\theta)C_{nI^2}\times\phi_{Airy} \quad (13)$$

$$\sigma_{IR}=0.132\pi^2k^2\int_0^L dz\int_0^\infty dKK\Phi_s(K)\sin(2\theta)C_{nIR}\times\phi_{Airy} \quad (14)$$

with

$$C_{nR^2}=\frac{A_T{}^2}{\langle T\rangle^2}C_{T^2}+\frac{A_q{}^2}{\langle q\rangle^2}C_{q^2}+2\frac{A_T A_q}{\langle T\rangle\langle q\rangle}C_{Tq} \quad (15)$$

$$C_{nI^2}=\frac{B_q{}^2}{\langle q\rangle^2}C_{q^2} \quad (16)$$

$$C_{nIR}=\frac{B_q A_q}{\langle q\rangle^2}C_{q^2}+\frac{B_q A_T}{\langle T\rangle\langle q\rangle}C_{Tq} \quad (17)$$

The Bowen ratio can be used to simplify these equations: $\beta = \frac{c_p}{L_v}\frac{\sigma_T}{\sigma_q} = \frac{c_p}{L_v}\sqrt{\frac{C_{T^2}}{C_{q^2}}}$, where c_p is the heat capacity of air, L_v is the latent heat, and σ_T and σ_q are the standard deviations of T and q, respectively (for detailed description, see Moene 2003). Moreover, temperature and specific humidity are often highly correlated, so the correlation coefficient between T and q is usually assumed to be equal to ± 1 depending on atmosphere stability. However, this assumption is verified only for |β|>0.1 (Lüdi et al., 2005, Solignac, 2009b). Then:

$$\frac{C_{TQ}}{\langle T\rangle\langle q\rangle} \approx \pm\sqrt{\frac{C_{q^2}}{\langle q\rangle^2}\frac{C_{T^2}}{\langle T\rangle^2}} \quad (18)$$

As such, the ratio of each variance at a given wavelength, and for a given set up, is dependent on the choice of the turbulent spectral behaviour $\Phi_s(K)$, and the values of C_{nR^2} and C_{nIR} (mainly controlled by β values). C_{nI^2} has a minor influence as variations in B_q compensate variations in q, and C_{q^2} disappears when calculating the ratio between each variances.

APPENDIX B

Calculation of the theoretical density power spectrum of the real and imaginary parts of the log amplitude fluctuations

This appendix aims to describe the expression of the theoretical density power spectrum of the different phenomena observed by a scintillometer. This expression was described for large aperture by Nieveen et al. (1998) and can be found in several previous studies for small aperture (Lee and Harp 1969; Clifford et al. 1971; Hill et al. 1980).

$$PSD_R = 16\pi^2 k^2 \int_{\frac{2\pi f}{v}}^{\infty} dK \int_0^L dz K \Phi_R(K) \sin^2\left(\frac{K^2 z(L-z)}{2kL}\right) \phi_{Airy} F_{Freq} \quad (19)$$

$$PSD_I = 16\pi^2 k^2 \int_{\frac{2\pi f}{v}}^{\infty} dK \int_0^L dz K \Phi_I(K) \cos^2\left(\frac{K^2 z(L-z)}{2kL}\right) \phi_{Airy} F_{Freq} \quad (20)$$

$$PSD_{IR} = 16\pi^2 k^2 \int_{\frac{2\pi f}{v}}^{\infty} dK \int_0^L dz K \Phi_{IR}(K) \sin\left(\frac{K^2 z(L-z)}{kL}\right) \phi_{Airy} F_{Freq} \quad (21)$$

with $\phi_{Airy} = \left\{ \frac{2J_1(\frac{KDz}{2L})}{\frac{KDz}{2L}} \right\}^2 \left\{ \frac{2J_1(\frac{KD(L-z)}{2L})}{\frac{KD(L-z)}{2L}} \right\}^2$

and $F_{Freq} = \left[(Kv)^2 - (2\pi f)^2 \right]^{-\frac{1}{2}}$

References

Avila, R., Vernin, J. and Masciadri, E. (1997) Whole atmospheric-turbulence profiling with generalized scidar. *App. Opt.*, **36**: 7898-7905

Beziat, P., Ceshia, E., and Dedieu, G., (2009) Carbon balance of three crop succession over two cropland sites in South-West France, *Agric. For. Meteorol.* **149**: 1628-1645.

Clifford, S.F., (1971) Temporal-Frequency Spectra for a Spherical Wave propagating through Atmospheric Turbulence, *J. Opt. Soc. Am.* **61**, 1285-1292.

De Bruin, H.A.R., Van den Hurk, B.J.J.M., and Kohsiek, W., (1995) The Scintillation Method tested over a dry vineyard area. *Boundary-Layer Meteorol.* **76**: 25-40.

Foken, T. (2008). Micrometeorology. Springer Verlag Germany.

Green, A.E., Green, S.R., Astill, M.S. and Caspari, H.W. (2000) Estimating Latent Heat Flux from a Vineyard using Scintillometry. *Terr. Atmos. Ocean. Sci.*, **11**: 525-542.

Hartogensis, O.K., Watts, C.J., Rodriguez, J.-C., de Bruin, H.A.R. (2003) Derivation of the effective height for scintillometers: La Poza experiment in Northwest Mexico. *J. of Hydrol.* **4**: 915-928.

Hill, R.J., Clifford, S.F. and Lawrence, R.S. (1980) Refractive index and absorption fluctuations in the infrared caused by temperature, humidity and pressure fluctuations. *J. Opt. Soc. Am.* **70:** 1192-1205.

Ingensand, H., (2002) Concepts and Solutions to Oversome the Refraction Problem in Terrestrial precision Measurement. FIG XXII International Congress, Washingtion, D.C. USA, April 19-26 2002: 12pp.

Irvine, M., Lagouarde, J.-P., Bonnefond, J.-M., Grimmond, S., and Oke, T.R. (2002) Spectral analyses of Optical Scintillations: Refraction and Absorption Components in an Urban Zone (Marseille, France), Proc. 4th AMS Symposium on Urban Environment, May 2002, Norfolk, VA, 217-221.

Kaimal, J., Wyngaard, J., Izumi, Y., and Cote, O. (1972). Spectral characteristics of surface layer turbulence. Q. J. R. Meteorolo. Soc., **98**:563:589.

Mis en forme : Anglais (Royaume-Uni)

Mis en forme : Anglais (Royaume-Uni)

Mis en forme : Anglais (Royaume-Uni)

Kleissl, J., Gomez, J., Hong, S.-H., Hendrickx, J.M.H, Rahn, T., and Defoor, W.L. (2008) Large Aperture Scintillometer Intercomparison Study. *Boundary-Layer Meteorol.* **128**:133-150.

Kleissl, J., Watts, C.J., Rodriguez, J.C., Naif, S., and Vivoni, E.R. (2009) Scintillometer Intercomparison study-continued. *Boundary-Layer Meteorol* **130**: 437-443.

Kolmogorov, A. (1941). Dissipation of energy in a locally isotropic turbulence. *C.R. Acad. Sci. URSS*, **32**, 16.

Lagouarde, J.P., Bonnefond, J.M., Kerr, Y.H., McAneney, K.J. and Irvine, M. (2002) Integrated sensible heat flux measurements of a two-surface composite landscape using scintillometry. *Boundary-Layer Meteorol.* **105**: 5-35.

Lee, R.W. and Harp, J.C. (1969) Weak scattering in Random Media, with Application to Remote Probing. *Proc. IEEE* **57**: 375-406.

Lüdi, A., Beyric, F. and Mâtzler, C., (2005) Determination of the Turbulent Temperature-Humidity Correlation from Scintillomtric Measurements, *Boundary-Layer Meteorol.*, **117**: 525-550.

McAneney, K.J., Green, A.E., and Astill, M.S., (1995) Large-Aperture scintillometry : the homogeneous case. *Agric. For. Meteorol.* **76**: 149-162.

Meijninger, W.M.L., Green, A.E., Hartogensis, O.K., Kohsiek, W., Hoedjes, J.C.B., Zuurbier, R.M., and de Bruin, H.A.R. (2002) Determination of area-averaged water vapour fluxes with large aperture and radiowave scintillometers over a heterogeneous surface-flevoland field experiment. *Boundary-Layer Meteorol.* **105**: 63-83.

Moene, A.F. (2003) Effects of water vapour on the structure parameter of the refractive index for near-infrared radiation. *Boundary-Layer Meteorol.*, **107**: 635-653.

Moene, A.F., Meijninger, W.M.L., Hartogensis, O.K., Heusinkveld, B.G., and de Bruin, H.A.R, (2005) The effectof finite accuracy in the manufactring of Large Apert-ure Scintillometers. Internal Report 2005/1, Meteorology and Air Quality Group, Wageningen University, Wageningen, the Netherlands, 19pp.

Nieveen J.P., Green A.E., Kohsiek W. (1998) Using a large-aperture scintillometer to measure absorption and refraction index fluctuations. *Boundary-Layer Meteorol.* **87**: 101-116.

Ochs G., Wilson J. (1993) A second Generation large-aperture scintillometer. *NOAA Tech. Memo. ERL WPL-232*: 31pp.

Qian, S. And Chen, D. (1993) Discrete Gabor Transform. *IEEE Trans. Signal Process.* **41**: 2429-2438.

Solignac, P.A., Selves, J.L., Béteille, J.P., and Gastellu-Etchegorry, J.P. (2007) Scintillometer data processing enhancement by Gabor transform and expansion. *Proc. IEEE IMTC, May 2007, Warsaw, Poland*: 4pp.

Solignac, P.A., Brut, A., Selves, J.L., Béteille, J.P., Gatsellu-Etchegorry, J.P., Keravec, P., Béziat, P., and Ceshia, E. (2009a) Uncertainty analysis of the computation methods to derive the sensible heat flux from scintillometer. *Atmos. Meas. Tech.* **2**: 741-753.

Solignac, P.A (2009b) Conception, Réalisation et Mise en oeuvre d'un scintillomètre: Influence de la vapeur d'eau dans la bande 940 nm. PhD Thesis, Université de Toulouse: 175pp.

Strohbehn J. (1968) Line-of-sight wave propagation through the turbulent atmosphere', *Proceedings of the IEEE*, **56**, 1301–1318.

Tatarskii V. I., (1961) *Wave Propagation in a Turbulent Medium*. McGraw Hill, 232 pp.

Vernin, J., Chadid, M., Aristidi, E., Agabi, A., Trinquet, H. and M. Van der Swaelmen (2009) First single star scidar measurements at Dome C, Antartica. *Astron. & Astrophys.* **500**: 1271-1276.

Mis en forme : Français (France)

Mis en forme : Anglais (Royaume-Uni)

List of Tables

TABLE 1. Theoretical evaluation of the underestimation of the variance, σ^2_R*(fixed band-pass)*-σ^2_R /σ^2_R, due to the use of fixed band-pass filtering, in comparison with a non filter variance, in absorption free conditions. Variance have been calculated thanks to the power spectrum density, PSD_R (Eq. 19), for various wind speed, by removing variance contribution located at frequencies under 0.1Hz, 0.2Hz or 0.5Hz.

	v=0.2 m.s^{-1}	**v=1 m.s^{-1}**	**v=2.5 m.s^{-1}**
0.1Hz	8.7%	1.6%	<1%
0.2Hz	17.6%	3.3%	1.3%
0.5Hz	43.6%	8.5%	3.4%

Figure captions

Figure 1 Transmittance of the atmosphere around 940 nm calculated using MODTRAN and, considering only the water vapour absorption (dotted line) and all attenuations (solid line) for L=300 m, HR = 50%, T = 293 K (in black) and for L = 2500 m, HR = 50%, T = 293 K (in grey). The emission diagram of the LED is also displayed (grey dashed line).

Figure 2 Contribution of absorption $(\sigma_{IR}+\sigma^2_I)/\sigma^2_R$ estimated from theoretical equations versus the Bowen ratio for various wind speed (0.5 and 5 m s^{-1})

Figure 3 Theoretical power spectrum density (PSD) of the log amplitude fluctuations in dry (left side) and wet (right side) conditions, with D = 15 cm, L = 300 m, v = 1 m s^{-1}, λ = 940 nm and C_{nR^2} = 2.63 10^{-14} $m^{-2/3}$. In dry conditions, C_{nIR} = 4.94 10^{-19} $m^{-2/3}$ and C_{nI^2} = 9.27 10^{-24} $m^{-2/3}$. In wet conditions, C_{nIR} = 4.94 10^{-18} $m^{-2/3}$ and C_{nI^2} = 9.27 10^{-22} $m^{-2/3}$. Contributions of the real and imaginary parts are plotted as PSD C_{nR^2} for the real part and PSD C_{nIR} + PSD C_{nI^2} for the absorption contribution. The transition frequency (f_T) between absorption and refraction is presented in the left side panel.

Figure 4 Power spectrum density of log amplitude fluctuations of the signal acquired from the LAS output on July 17 2008 1200 UTC (a.) and 18 UTC (b.). The dashed line corresponds to the PSD_R according to Eq. 19.

Figure 5 Theoretical power spectrum density of the log amplitude fluctuations of the signal acquired at the output of an LAS for various wind speed : 1 m s-1 (black line) 5 m s-1 (grey dashed line), according to Eq. 19 of Appendix B. All other parameters are the same : Cn² = 2.63e-14 m-2/3, D = 15cm, L = 565m and λ = 940nm.

Figure 6 Power Spectrum Density of the signal acquired from the LAS output on July 17 2008 1800 UTC. The original signal (solid black) corresponds to the signal with no filtering, the Gabor signal (solid grey) is the original signal filtered by Gabor filtering BP 0.1-400 Hz, and Tchebychev (dotted black), is the original signal filtered by a Tchebychev 2 filter BP 0.1-400 Hz of order 12.

Figure 7 Power Spectrum Density of the signal acquired from the LAS output on July 17 2008 800 UTC. The original signal (solid black) corresponds to the signal with no filtering, BP 0.1 400 Hz (dotted grey) is the original signal filtered by Gabor filtering BP 0.1 - 400 Hz, and Reconstructed (dashed grey) is the original filtered by Gabor filtering BP f_T-400 Hz, but where the coefficient outside the band pass are set to the refractive plateau value.

Figure 8 Comparison between C_{n^2} *LAS* from the LAS output 'C_{n^2}' and C_{n^2} calculated from the raw signal filtered by a Gabor BP filter 0.1-400 Hz.

Figure 9 a)Time series of a. the transition frequency, b). the demodulated signal (values of Demod > -100 mV are in a grey dashed line, and the other values are in a black solid line), c). ΔC_{n^2}= ([C_{n^2} (raw signal) – C_{n^2} (reconstructed)]/ C_{n^2} (reconstructed)) between August 2 and August 13 2008.

Figure 10 Relative difference ΔC_{n^2}= ([C_{n^2} (fixed band pass) – C_{n^2} (reconstructed)]/ C_{n^2} (reconstructed)) are plotted as a function of wind speed for various filters, in condition of negligeable absorption contribution . The various band-pass filters studied here are 0.1- 400 Hz (black circles), 0.2 - 400 Hz (white squares), and 0.5 - 400 Hz (grey circles).

Figure 11 Relative difference ΔC_{n^2}= ([C_{n^2} (fixed band pass) – C_{n^2} (reconstructed)]/ C_{n^2} (reconstructed)) is plotted as a function of wind speed for 2 BP filters, between August 2 and 13 2008. The various band-pass filters studied here are 0.1- 400 Hz (black circles), 0.2 - 400 Hz (white squares).

Figure 12 Relative differences ΔC_{n^2} = ([C_{n^2} (adaptive band-pass) – C_{n^2} (reconstructed)]/ C_{n^2} (reconstructed)) are plotted as a function of wind speed for an adaptive filtering, between August 2 and 13.

Figure 13 On the left side, normalized energy turbulent spectrum of q (grey lines) and T (black lines). On the right side, power spectrum of log amplitude fluctuations of the signal recorded at the output of an LAS. Three cases are presented here for July 5 : 730 (a. and d.), 1400 (b. and e.) and 2000 (c. and f.) UTC.